Polymerization of cyanoacetylene under pressure: Formation of carbon nitride polymers and bulk structures

Mohammad Khazaei,* Yunye Liang, Natarajan S. Venkataramanan, and Yoshiyuki Kawazoe
Institute for Materials Research, Tohoku University, Sendai 980-8577, Japan
(Received 22 September 2011; revised manuscript received 26 December 2011; published 1 February 2012)

High-pressure phase transitions of polar and nonpolar molecular structures of cyanoacetylene (HC_3N) are studied by using first-principles simulations at constant pressure. In both polar and nonpolar crystals, at pressure ∼20 GPa, the cyanoacetylene molecules are interconnected together and form polyacrylonitrile (PA) polymers. At pressure ∼30 GPa, PA polymers are transformed to polymers with fused pyridine rings (FPR's). The individual geometrical structures of PA and FPR polymers obtained from polar and nonpolar molecular crystals of cyanoacetylene are identical, but their stacking is different. At pressures above 40 GPa, the FPR polymers are interconnected together and new three-dimensional (3D) carbon nitride systems are formed. At ambient pressure, the long-length PA and FPR polymers are metallic, and the created 3D structures are an insulator with energy band gaps around 2.85 eV. The electron transport characteristics of FPR polymers with different lengths are investigated at finite biases by using the nonequilibrium Green's function technique combined with density functional theory (DFT) by connecting the polymers to gold electrodes. The results show that FPR polymers have negative differential resistance behavior. Our time-dependent DFT calculations reveal that FPR polymers can absorb light in the visible region. From our results, it is expected that the FPR polymers will be a good material for optoelectronic applications.

DOI: 10.1103/PhysRevB.85.054101 PACS number(s): 61.50.Ks, 61.66.Fn, 73.63.−b

I. INTRODUCTION

Widespread technological applications of conjugated polymers in solar cells,[1] rechargeable batteries,[2] supercapacitors,[3,4] and electronic and spintronic nanodevices[5–8] have led to many theoretical and experimental investigations that have been devoted to synthesis, characterization, and functionalization of conjugated polymers. Polymers are generally prepared and functionalized in solutions with the use of appropriate catalysts to obtain macromolecular materials with well-defined rigid structural arrangements. It has been shown that the mechanical, electronic, and physical properties of polymers depend a great deal on their sizes, geometries, and regularities.[9–13] Along with the conventional catalytic methods in the preparation of functionalized polymers, the high-pressure techniques offer the possibility of polymerization in the absence of solvents or catalysts. In the latter, the high pressure is considered to be an alternative to catalytic effects to prepare well-defined polymeric materials.[14]

Among various conjugated polymers, polyacetylene and polyacenes with one-dimensional structures were of scientific interest due to their wide applications.[15,16] Polyacetylene is a very simple conjugated polymer, consisting of a linear backbone of carbon atoms, in which each carbon atom is bonded to one hydrogen. Polyacenes belong to a class of polyclick aromatic hydrocarbon polymers and are planar with sets of linearly fused benzene rings. It has been shown that the electronic properties of polyacetylene and polyacenes alter when the hydrogen atoms are replaced with other elements or ligands.[17–22] In this regard, Aoki *et al.* have reported experimental observations on the polymerization of cyanoacetylene molecules (HC_3N) at pressures above 1.5 GPa into a polyacetylene-like chain, in which every second hydrogen atom has been replaced with a cyano group (CN),[23] called polyacrylonitrile. By using first-principles calculations, Springborg studied the electronic structure of polyacrylonytrile (PA) and compared its stability with a polymer with the same composition, consisting of fused pyridine rings (FPR's), similar to polyacene structure. Springborg found that FPR polymer has a lower total energy than PA polymer, and they are both semiconductors.[19,20]

In the present study, by performing a set of first-principles calculations, we have investigated the phase transitions of polar and nonpolar molecular crystal structures of cyanoacetylene under pressure from 0 to 55 GPa. From our calculations, it turns out that at pressures around 20 GPa, cyanoacetylene molecules are polymerized into a one-dimensional CN polymer, PA, as suggested by Aoki *et al.*, and when the pressure is increased to above 30 GPa, the former polymer is transformed into an FPR. At high pressures above 40 GPa, the FPR polymers are connected together and form an insulating three-dimensional (3D) carbon nitride solid. When the pressure is released, the geometrical structure of the FPR polymer with fused rings is less distorted than that of the PA. This makes it possible to connect the FPR polymer to the metal electrodes for electronic applications. In this regard, we have examined the *I-V* characteristics of FPR polymers with different numbers of pyridine rings at finite biases by connecting them to the gold electrodes by using the nonequilibrium Green's function formalism combined with first-principles calculations. We have also studied the light absorbance behavior of FPR polymers using the time-dependent density functional theory (TDDFT) method to examine their possible applications in optoelectronic devices.

II. METHOD OF CALCULATIONS

All the calculations are carried out within the context of density functional theory (DFT) using the Perdew-Burke-Ernzerhof (PBE) exchange-correlation functional,[24] with the split valence double-ζ plus polarization orbitals basis set, and the norm-conservative Troullier-Martins pseudopotential[25] as

implemented in the SIESTA package program.[26–28] A uniform mesh grid, with an equivalent plane-wave cutoff of 500 Ry, is used to represent the electron density, the local part of the pseudopotentials, and the exchange-correlation potential. The corresponding Brillouin zone is sampled by a set of $6 \times 6 \times 6$ Monkhorst-Pack k points.[29] For structural optimizations, a variable-cell-shape conjugate gradient method under constant pressure is used without any constraint on symmetry. At the given pressure, the cell shape, volume, and atomic positions are optimized until the magnitude of force on each atom becomes smaller than 0.005 eV/Å. The stress tolerance is 1.0 GPa. The reliability of the SIESTA code in predicting new phases under high pressure has already been proved in many different studies.[30,31]

To find the transition structures, the molecular structure of cyanoacetylene molecules is optimized using the variable-cell-shape conjugate gradient method under a constant pressure as described above. In order to find other possible transformations and prevent overestimation of the transition pressures, we have performed additional calculations; after applying pressure in each step of the simulation, we distorted the supercell, displaced atoms slightly from their optimized positions randomly, and reoptimized the structure once again.[32,33]

For the electron transport calculations, the polymer structures are connected to gold (111) leads using sulfur atoms. The nonequilibrium Green's function (NEGF) technique combined with density functional theory is used to obtain the I-V characteristics. We have used the GGA-PBE functional with the double-ζ plus polarization basis set for the atoms in the polymers and the single-ζ plus polarization basis set for the gold atoms in the leads. The calculations are carried out with a commercial package, Atomistix ToolKit (ATK).[27,34–36]

The optical calculations have been done using the PBE0 (also known as PBE1PBE) exchange correlation functional as implemented in the GAUSSIAN G09 suite of programs and the 6-311++G(d,p) basis set.[37] This functional is based on the generalized gradient functional PBE by mixing 25% of Hartree-Fock exchange, calculated with Kohn-Sham orbitals, and 75% of PBE exchange, and it uses the PBE correlation functional.[38,39] Furthermore, studies have shown that the use of PBE0 can provide reasonable estimates of the color of organic dyes and is adequate to treat molecules with delocalized excited states.[40]

III. RESULTS AND DISCUSSION

Cyanoacetylene, H−C≡C−C≡N, exhibits a conjugated system with an electrical dipole moment of 3.6 ± 0.2 D.[41] The experimental molecular crystalline structure of cyanoacetylene at 25 °C is monoclinic, including two molecules per unit cell with a likely space group of $P2_1/m$, $P2_1$, or Pm.[42] In the molecular crystals with $P2_1/m$ and $P2_1$ group symmetries, the molecules in the cell would have to be oriented in opposite directions, but they could be oriented alike in Pm. In the refinement process of the experiments performed by Shallorss and Carpenter, test structures in Pm with two parallel molecules gave decidedly poorer agreement than the corresponding antiparallel arrangement.[42] Hence, Shallorss and Carpenter assumed that the most probable space group for cyanoacetylene is $P2_1/m$, and they refined the geometrical parameters by assuming this symmetry; see Table I.[42] The molecules in crystals with Pm and $P2_1/m$ symmetries are joined together by C−H···N hydrogen bonds, resembling linear infinite parallel chains. All the molecules in a given chain are oriented alike. Since cyanoacetylene (HC_3N) is a polar molecule, Pm crystal with molecules in the same orientations is a polar crystal and $P2_1m$ crystal with molecules oriented oppositely is nonpolar. In this study, we have investigated both of the above polar and nonpolar crystals. It is observed that at zero pressure, both polar and nonpolar crystals of cyanoacetylene are monoclinic. As seen from Table I, the geometrical structures and parameters of these molecular crystals are very similar and are in good agreement with the experimental data. Even their total energy difference is very negligible, less than 0.01 eV/mol (while Pm is more stable). Hence, with such a small energy difference between Pm and $P2_1/m$ crystals, we cannot strictly conclude which of them is the most favorable structure. Hence, it became essential to study the phase transitions of both polar and nonpolar crystals under pressure in detail.

A. Phase transitions under pressure

Figure 1 shows the pressure dependences of the enthalpy and volume of the polar and nonpolar molecular crystals of cyanoacetylene when the external pressure is changed from 0 to 55 GPa. The enthalpy is defined as $H = E_{\text{tot}} + PV$, where E_{tot}, P, and V are the total energy, pressure, and volume of the unit cell, respectively. ΔH represents the relative enthalpy of the systems at certain pressure to the enthalpy of the same system at zero pressure. From enthalpy curves, it is observed that under pressure, both polar and nonpolar HC_3N systems obtain several first-order transitions. The polar crystal has first-order transitions at 20, 30, and 40 GPa. The nonpolar one has first-order transitions at 16, 30, and 45 GPa. All the phase transitions are simultaneous with sudden contractions of volumes. The structures corresponding to phase transitions are shown in Fig. 2. From Figs. 1 and 2, it is seen that under pressure, polar and nonpolar crystals of HC_3N at first are

TABLE I. The lattice parameters (Å), angles (degree), and bond distance (Å) of polar (with Pm group symmetry) and nonpolar (with $P2_1/m$ group symmetry) molecular crystals of cyanoacetylene at zero pressure.

	a	b	c	α	β	γ	C≡N	C−C	C≡C	C−H
Experiment[a]	6.96	6.30	3.84	90.0	110.5	90.0	1.14	1.38	1.18	0.95
Polar molecular crystal	6.81	5.64	3.61	90.0	120.6	90.0	1.18	1.38	1.24	1.11
Nonpolar molecular crystal	6.82	5.60	3.48	90.0	116.9	90.0	1.18	1.38	1.24	1.11

[a]Reference 42.

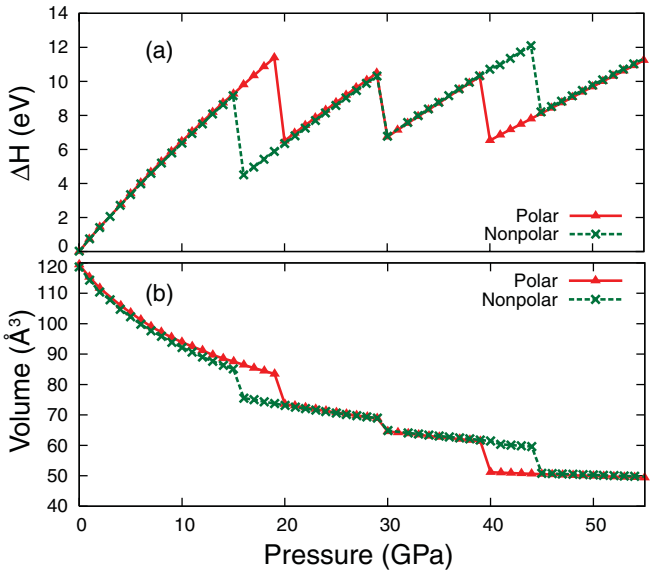

FIG. 1. (Color online) Pressure dependences of enthalpy (a) and volume (b) of polar and nonpolar molecular crystal of cyanoacetylene.

transformed to PA polymers and then are transformed to polymers with fused pyridine rings, FPR polymers, and then to three-dimensional CN solids. The coordinates of the transition structures are presented in the supplemental material.[43]

The unit cells of polar and nonpolar molecular crystals of cyanoacetylene have two molecules per cell. Hence, upon applying pressure, each unit cell results in two individual polymers. The geometrical structures of the individual polymers formed after applying pressure on polar and nonpolar molecular crystals are identical [see Fig. 2(a)], but the way they are stacked is different. In the unit cells of PA and FPR polymers that result from polar molecular crystal, the directions of all C−H bonds of the two polymers in the unit cell are parallel and are in the same direction; see Fig. 2(b). In the unit cells of PA and FPR polymers, which result from nonpolar molecular crystal, the C−H bonds of the two polymers in the unit cell are parallel but are in opposite directions; see Fig. 2(c). From our simulations, it is seen that the polymerization proceeds when the HC_3N molecules are connected to their lateral neighboring molecules with the same directions as the C−H bond (the same directions of dipole moments). This is the reason why in any of the individual polymers, all the C−H bonds are in the same direction. From the relative locations of polymers in the unit cells, it is observed that the polymers adjust their locations such that the directions of their C−H bonds are oriented toward the N atoms of the lateral neighboring polymer, so as to form C−H· · ·N hydrogen bonds. We have repeated the above calculations with larger supercells consisting of eight HC_3N molecules, and we found the same polymers.

By applying higher pressures above 40 GPa, the polymers with fused rings are connected together to form a new

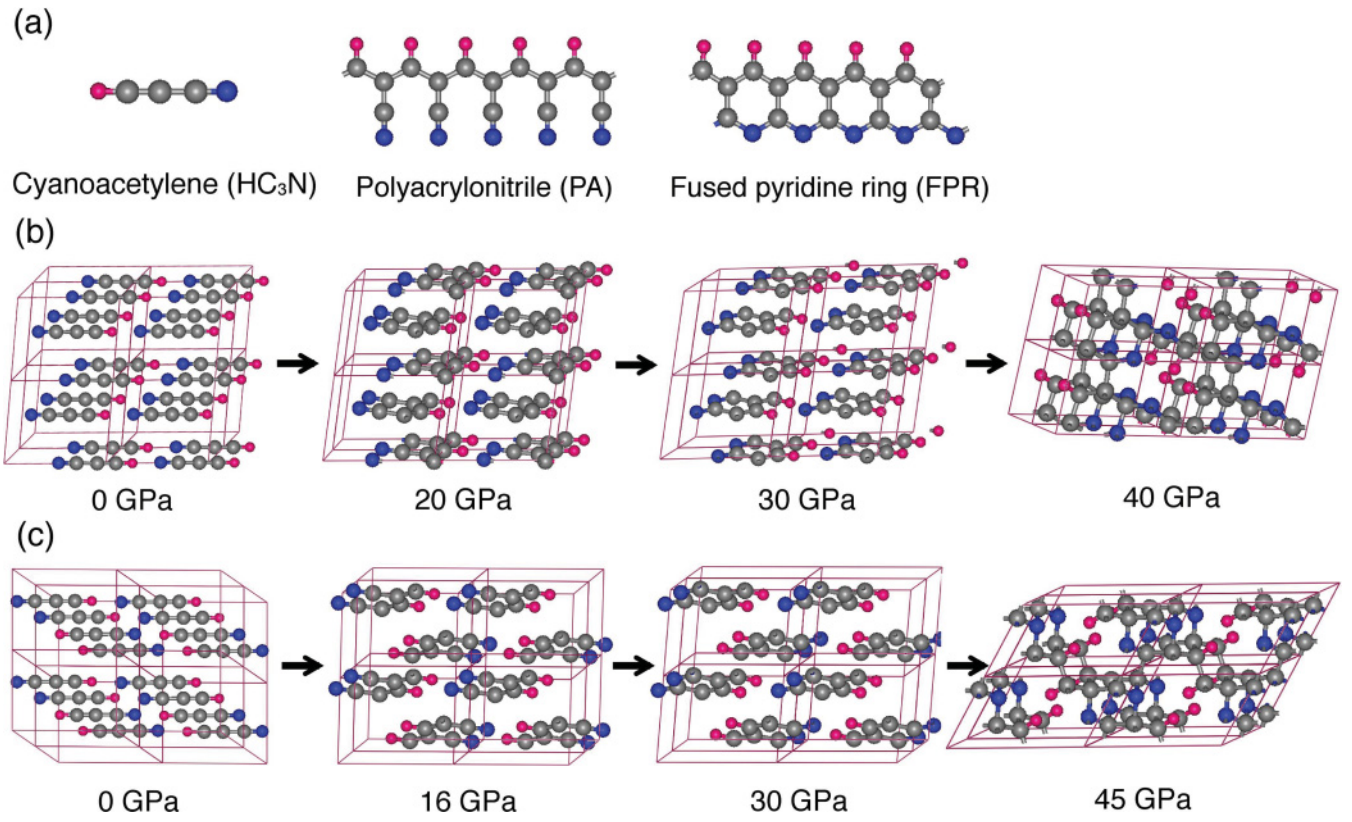

FIG. 2. (Color online) The molecular structure of cyanoacetylene, polyacrylonitrile, and fused pyridine ring polymers are shown in (a). The transition structures of polar and nonpolar molecular crystal of cyanoacetylene are depicted in (b) and (c), respectively. Pink, gray, and blue balls represent the hydrogen, carbon, and nitrogen atoms.

three-dimensional solid; see Figs. 2(b) and 2(c). As the stacking of FPR polymers in the polar and nonpolar crystals is different, their resultant 3D solids are different. In both structures, all the nitrogen and carbon atoms are threefold- and fourfold-coordinated, respectively. For a better understanding of the mechanism of the formations of polymers and solids from cyanoacetylene molecules, we have provided the trajectories of formations in the supplemental material.[43] It should be noted that in first-principles simulations, the phase-transition pressures are typically overestimated in comparison to the experiments, which is mainly due to neglecting the experimental conditions (temperature and time length of experiments) in the calculations. This issue has been well discussed in our previous studies[30,31] and in the studies by other groups.[44,45]

In order to consider the relative stabilities of the created structures at different pressures, we have calculated the enthalpy-pressure curves of the predicted structures. For this, first we performed a set of total energy calculations to obtain the energy versus volume curves by keeping the symmetries of the structures fixed during the optimization process. Then from the above calculations, we extracted the typical enthalpy ($H = E_{\text{tot}} + PV$, $P = -\Delta E/\Delta V$) versus pressure curves. Since the 3D, FPR, and PA products of polar and nonpolar molecular structures of HC_3N are very similar, the general behaviors of their E-V and H-P curves are also very similar. Hence, we have just shown the energy and enthalpy curves of the products of polar molecular crystal with PM symmetry in Fig. 3, and the curves related to the nonpolar crystal are added to the supporting information file.[43] From E-V curves, it is observed that the equilibrium volumes of the created 3D structures are smaller than the FPR polymers $<$ PA polymers and smaller than the volumes of the molecular crystals of HC_3N. It is also observed that the 3D structures (~ -3.50 eV/mol) $<$ FPR polymers (~ -3.10 eV/mol) $<$ PA polymers (~ -1.66 eV/mol) are energetically much more stable than gas molecules (0.0 eV/mol) at zero pressure. From H-V, it is observed that at positive pressures, the 3D structures are more stable than FPR and PA polymers and the gas molecular crystal. At negative pressures between -5 GPa and 0, the 3D structure is the most stable structure. At pressures between -20 and -5 GPa, the FPR polymers are the most stable structures. At higher negative pressures, the PA polymers are the ones that are stable. In our previous calculations, we showed that under positive pressures, the molecular crystals of HC_3N are transformed to PA polymers $\rightarrow$ FPR polymers $\rightarrow$ 3D structures. Conversely, from the above set of calculations, it is observed that at negative pressures when the formed structures are stretched, the 3D structures are transformed to FPR polymers$\rightarrow$ PA polymers as seen from the intersections of the enthalpy curves. It is obtained that at -5 GPa, the 3D structure can be transformed to FPR polymers, and at around -20 GPa, the FPR rings can be transformed to PA polymers. In the experiments, zero pressure is the minimum pressure that can be applied on the molecules in a molecular crystal. Therefore, it can be deduced that after the formations of the 3D, FPR, and PA structures, there is almost no possibility that they will retransform to the molecular gas structures at zero temperature.

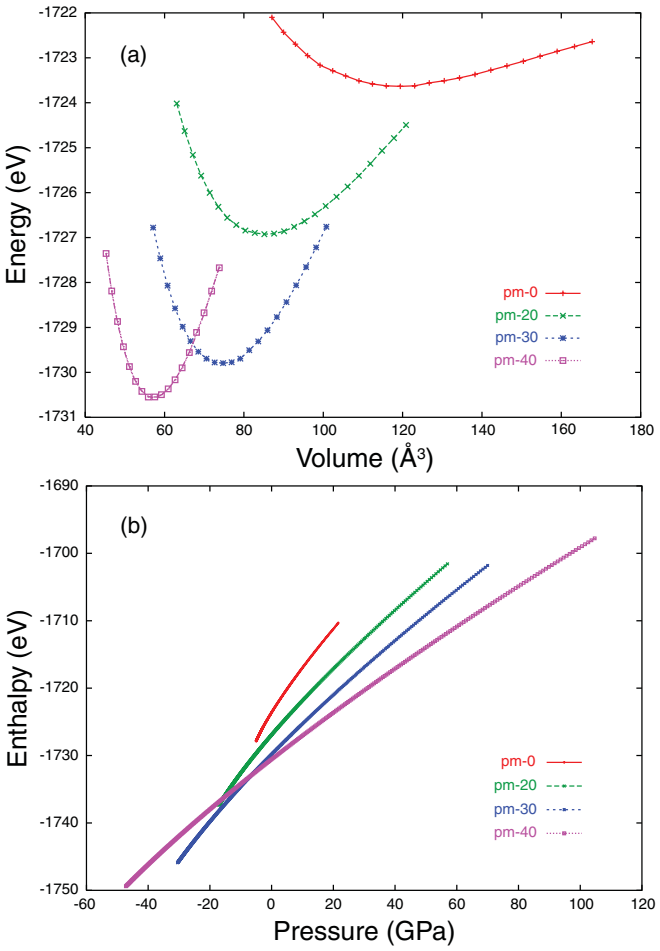

FIG. 3. (Color online) The relative stabilities of the products of polar crystal of HC_3N with Pm symmetry are considered at different volumes and pressures through their energy-volume and enthalpy-pressure curves in (a) and (b). The curves related to nonpolar crystal are added to the supporting information file.[43]

In order to consider the geometrical and electronic structures of designed polymers at ambient pressure, we have prepared very long polymers with a length of 35 Å, and we optimized them in very large supercells ($50 \times 50 \times 50$ Å^3) until the magnitude of force on each atom became smaller than 0.01 eV/Å. The optimized structures are shown in the supplemental material.[43] It is observed that the PA polymer is significantly distorted to a helical-like shape. In PA, there is no binding between cyanide groups of the polymer, hence the cyanide groups adjust themselves in a helical shape to reduce the steric repulsion between their lone pair electrons on nitrogen atoms. However in FPR, the cyanide groups are not free. They are connected by C$-$N bonds to the two neighboring cyanides. Hence, the FPR polymer is less distorted, but it is curved because the C$-$N bonds ($\sim$1.35 Å) are shorter than the C$-$C bonds ($\sim$1.41 Å). From our calculations, it is observed that there are no significant changes in the geometries of the 3D CN solids when the pressure is released to zero, and their geometries are retained.

Figure 4 indicates the electronic structures of the long distorted PA and FPR polymers and the formed 3D structures at zero pressure. For comparison, we have also optimized

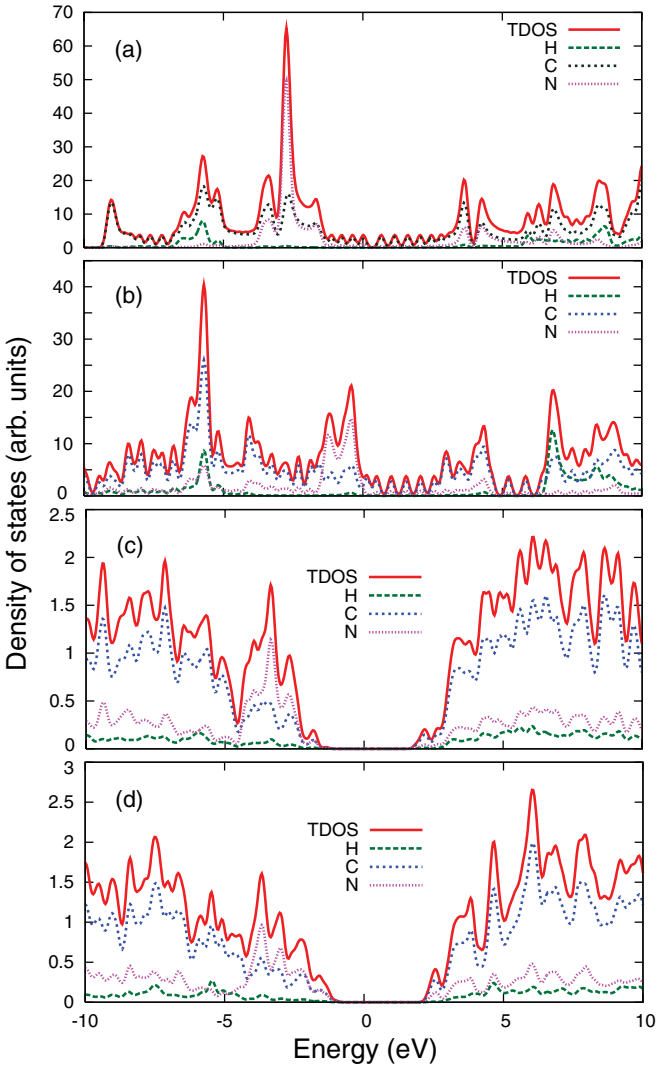

FIG. 4. (Color online) Total (TDOS) and projected density of states of a long PA and a long FPR polymer with 35 Å length are shown in (a) and (b), respectively. The optimized structures of these polymers are included in the supplemental material.[43] TDOS and projected density of states of the 3D structures obtained from polar and nonpolar molecular crystals are shown in (c) and (d).

the PA and FPR polymers under periodic conditions. In the periodic calculations, the polymers are partly optimized due to boundary conditions. It is observed that the studied polymers are semiconducting, as already reported by Springborg,[18–20] but when there is no constraint on the polymers, they are metallic near the Fermi energy. The 3D solid obtained from polar and nonpolar molecular crystals is an insulator with very large energy band gaps (2.9 and 2.8 eV, respectively), which are suitable for optical applications. From the projected density-of-state analysis, it is found that in an FPR and the 3D structures, the highest occupied energy states are mainly localized on C−N bonds, while the highest unoccupied states are localized on C−C bonds. As suggested by Springborg, if there is any electron excitation in these systems, there will be a charge separation in them.[20] This charge separation might increase the recombination time of holes and electrons such that these carriers can travel to the positive and negative electrodes and generate current without being recombined. This indicates that FPR polymers might be good candidates for organic-based solar cell materials. In the following sections, we will investigate the above idea by examining the electron transport and optical properties of FPR polymers.

When the phase-transition structures of cyanoacetylene (HC_3N) are compared with other gas molecules such as hydrogen cyanide (HCN),[31] benzene (C_6H_6),[46,47] cyanogen (C_2N_2),[30] carbon monoxide (CO),[48] and carbon dioxide (CO_2),[49] it is found that in the hydrogen-rich systems (HCN and C_6H_6), all the predicted structures are chainlike or layered. The hydrogen atoms prevent the interconnection between the layers. In the systems without hydrogen or with fewer hydrogen atoms, such as HC_3N, there are possibilities to find structures with three-dimensional networks.

It is worth mentioning that recently a dense tetrahedrally bonded phase of HC_2N_3 structure was experimentally synthesized by laser heating from dicyandimaide ($H_4C_2N_4$) at high pressure in a diamond anvil cell.[50,51] The obtained bulk moduli from experiment and DFT calculations are in good agreement, 258 ± 21 GPa.[50–52] We have also estimated the bulk modulus of our predicted three-dimensional structures by fitting the curves of total energies versus volume to the third-order Brich-Murnagahan equation of states.[53] It is found that our designed structures obtained from molecular crystals of HC_3N with Pm and $P2_1/m$ symmetries also have similar high bulk moduli of 258 and 270 GPa, respectively.

To consider the effect of van der Waals interactions on the results, we used the Grimme method implemented in the SIESTA code.[54] The necessary Grimme parameters have been taken from the original paper by Grimme.[54] As seen from Table I, our pure DFT calculations with localized basis sets underestimate the lattice parameters in comparison to the experimental results. When we included the van der Waals interactions, the attraction forces between the molecules increased, which resulted in a decrease in the lattice parameters once again; see the supporting information file.[43] We observed that by adding the dispersion effect into our DFT calculations, our results were not improved in comparison to the experiments. We also considered the effect of van der Waals interactions on the phase-transition pressures. We discovered that there are very slight changes in the phase-transition pressures, lowered by 2 GPa, in comparison to pure DFT calculations.

B. *I-V* characteristics of the FPR polymers

Since the FPR polymers are less distorted than the PA polymers, it is possible to connect them to metal electrodes. In order to obtain the electron transport properties of the FPR polymers, we have connected them to the gold leads through sulfur atoms. The sulfur atoms serve as alligator clips.[55] The sulfur atoms sit on the hollow or bridge sites of the nearest-neighboring gold atoms of the (111) surface with Au−S bond distances of ∼2.1 Å. After connecting each polymer to the gold leads [see the inset of Fig. 5(a)], the whole system can be divided into three parts: the left lead, the polymer, and the right lead. Because of the difference between the chemical potentials of the gold atoms and the polymer, the polymer is charged. Hence, to consider the interaction between

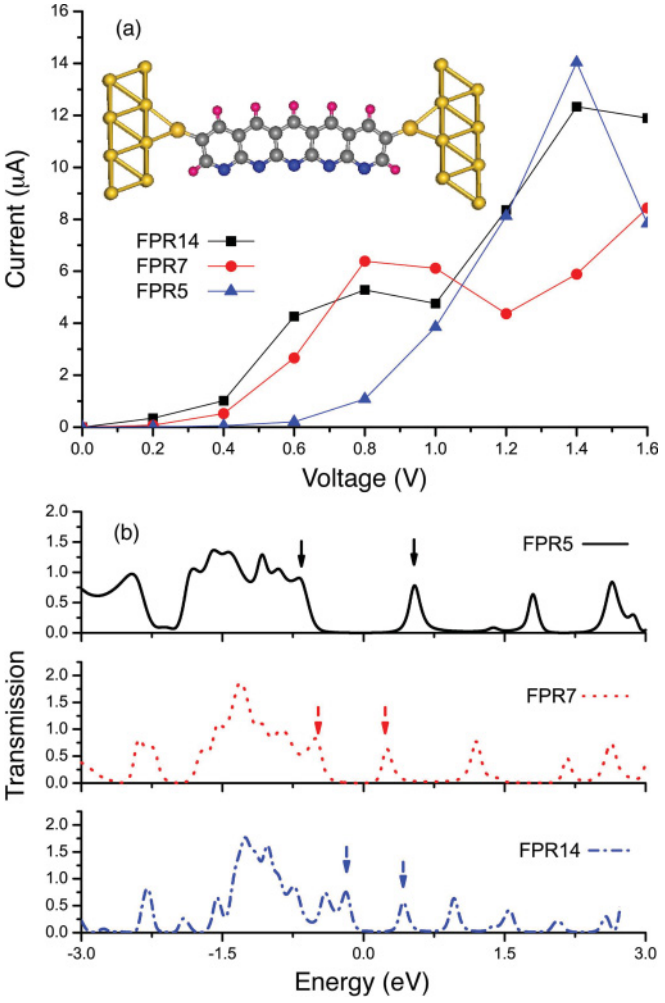

FIG. 5. (Color online) *I-V* characteristics of FPR polymers with different numbers of rings (5, 7, and 14) are shown in (a). The inset shows a typical FPR polymer connected by sulfur atoms to the gold electrodes. (b) indicates the transmission curves at zero voltage for the FPR 5, 7, and 14 polymers. The arrows show the position of HOMO and LUMO frontier orbitals. The *I-V* characteristics of FPR*n* ($n = 5$ to 14) are added to the supplemental material.[43]

the polymer and the leads accurately, two buffer layers of gold atoms on both sides of the leads are included in the polymer, thus forming an extended polymer.

The current is calculated from the Landauer-Büttiker formalism as

$$I(V) = (2e/h)\int_{-\infty}^{\infty} \mathrm{d}E\,T(E,V)[f(E-\mu_l) - f(E-\mu_r)], \tag{1}$$

where f is the Fermi function with electrochemical potential $\mu_{l,r}$. The chemical functions of the left and right leads are defined as $\mu_{l,r} = E_f \mp eV/2$, where E_f is the Fermi energy. $T(E,V)$ is the transmission probability of electrons with energy E from one lead to another lead through the polymer junction under an external bias V. At low temperature, this equation can be simplified as

$$I(V) = (2e/h)\int_{\mu_l}^{\mu_r} \mathrm{d}E\,T(E,V). \tag{2}$$

The *I-V* curves of FPR polymers with 5 to 14 rings (defined as FPR*n*, $n = 5$ to 14) are calculated. The current results of FPR5, 7, and 14 are shown in Fig. 5(a). The others are included in the supplemental material.[43] It is found that by increasing the length of polymers, the *I-V* characteristic of the FPR polymer changes gradually. For the short polymers, for example FPR5 [see Fig. 5(a)] at low voltage (< 0.4 V), the current is extremely small and proportional to the voltage. By increasing the voltage, the current increases exponentially. If the voltage is further increased (> 1.4 V), the current decreases, which indicates the negative differential conductance. By comparing the transport properties of FPR5 in Fig. 5(a) with longer polymers (for instance, FPR7), two main differences are observed. The threshold of the exponential increase becomes small (< 0.2 V) and the current begins to decrease at 0.8 V. It is found that the current increases again when the applied voltage is greater than 1.2 V. The *I-V* characteristic of FPR14, which is the longest polymer in this study, is also depicted in Fig. 5(a). It is found that at low voltage, the current is nonzero, which means that FPR14 is metallic. The negative differential conductance occurs at 0.8 V, but its peak-to-valley ratio reduces significantly. The current increases again after 1.0 V.

To understand the transport properties of FPR polymers, the transmission probabilities are calculated. The transmission results of FPR5, 7, and 14 at zero voltage are shown in Fig. 5(b). In transmission curves, every transmission peak indicates the existence of a tunneling channel. It can be easily found that the gaps between the highest occupied molecular orbital (HOMO) and the lowest unoccupied molecular orbital (LUMO) are the converse of the length of the polymers, and by increasing the length, the frontier orbitals get closer to the Fermi level. The energy levels of HOMO and LUMO frontier orbitals are shown by arrows in Fig. 5(b). The transmission probability of FPR5 at the Fermi level is very small, while the HOMO and LUMO are far away form the Fermi level. At low external voltage, the current flowing through the FPR5 is very small (almost zero). For FPR7, the transmission probability at the Fermi level is small, however its LUMO gets closer to the Fermi level, and this orbital can serve as a tunneling channel and contribute to the electron current when the external voltage is applied. The situation changes significantly for FPR14. From Fig. 5(b) we can find that in this case, the HOMO is the tunneling channel at the low external voltage, and the tail of the HOMO is crossing the Fermi level, which results in a metallic behavior of FPR14.

When external voltages are applied, the systems are in nonequilibrium. The electrons are redistributed in the junction and the charging effect takes place.[56,57] When the junctions are charged, the energy levels are broadened and shifted. The broadening comes from the hybridization of the molecular energy levels with the energy bands of the leads, which is related to the interaction between the polymer and the leads. The electrons flowing into the junction change the repulsion energy between the electrons and result in the shifts of the broadened energy levels. We have considered the transmission probabilities of FPR5 at different external voltages. The results are shown in the supplemental material.[43] At low voltages, the position and the corresponding transmission height of the LUMO change slightly. The position of the HOMO does not change, however the corresponding transmission height reduces gradually. The HOMO-LUMO gap is almost fixed. Since

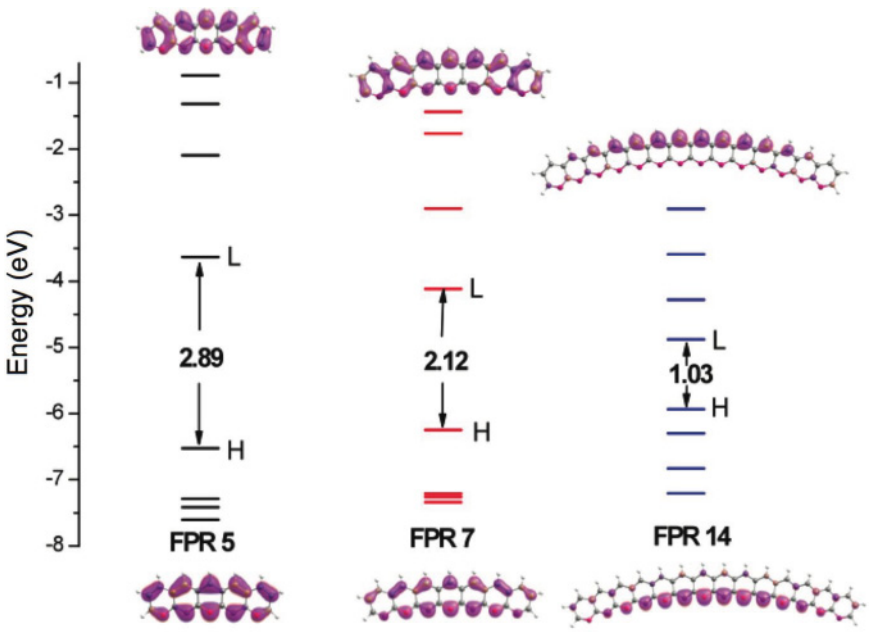

FIG. 6. (Color online) Schematic representation of the energy levels of the FPR 5, 7, and 14 polymers. Isodensity surface plots of HOMO and LUMO molecular orbitals are also shown.

the current is determined by the integration of transmission probability over an energy window from one quasi-Fermi-level to another, the current increases exponentially as the tails of the frontier orbitals enter into the integration window and serve as the tunneling channel. The occurrence of negative differential conductance at higher external voltages results from the reduction of transmission from the HOMO. By comparing the transmission curves at low voltages with those at higher voltages, some significant differences are observed. For example, the peak positions of the HOMO and LUMO shift toward the lower energy, and the height of transmissions from the HOMO and LUMO are reduced significantly. Therefore, in the NDR behavior of FPR polymers, two factors compete with one another and play important roles: the enlargement of the integration window increases the current, and the reduction of transmission from the HOMO decreases the current. As the latter overwhelms the former, the negative differential occurs. The same effect can be observed in longer polymers, therefore their behaviors are similar. The only difference is that the longer polymers have smaller HOMO-LUMO gaps, consequently the negative differential conductance and the rapid increasing of current can be found at lower voltages.

C. Optical property of FPR polymers

We have explored the absorption spectra of the FPR polymers in the vapor phase at the TDDFT/PBE0 level of theory. Prior to the TDDFT calculations, the structures are reoptimized using PBE0 and the 6-311++G(d,p) basis set. In general, the optical properties are governed by the frontier molecular orbital (FMO) components, the HOMO and LUMO energy levels, and energy gaps.[58] The FMO compositions and energy levels for FPR5, 7, and 14 are shown in Fig. 6. As we mentioned in the preceding section, the HOMO-LUMO energy gaps decrease with the increase in the number of FPR rings, which is consistent with the order of introduction of the increased π conjugation. Furthermore, the HOMO energy levels were raised and the LUMO energy levels were significantly lower with the increase in the number of rings. The spatial distribution diagram for FPR5 and 7 reveals that the HOMO and LUMO orbitals are localized over the rings, while in FPR14, the HOMO is exclusively localized on the nitrogen atoms of FPR rings and the LUMO is localized over the carbon atoms. The raised HOMO energy and the lower energy levels in the LUMO would benefit the hole-transporting ability and the electron-injecting ability of the systems, respectively, while used in organic photovoltaic cells. The simulated absorbance spectra for the systems with 5, 7, and 14 rings are shown in Fig. 7. It is interesting to note that as the ring number increases, the absorbance wavelength increases. For FPR5, the observed longest absorption is localized at 373 nm, which is mainly due to the HOMO-3 orbital to the LUMO level and is attributed to the ligand-to-ligand charge transfer (LLCT). For FPR7, the longest absorption gets redshifted to 420 nm, with main contributions are from HOMO-5 to the LUMO level. In FPR14, the longest absorption at 887 nm has HOMO to LUMO+1 contributions and the intense absorption occurs

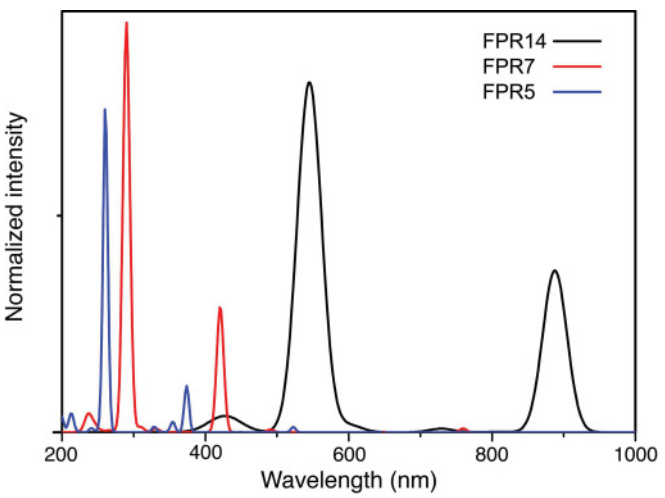

FIG. 7. (Color online) Simulated normalized absorption spectra for the FPR 5, 7, and 14 polymers.

at 546 nm. Furthermore, the calculated oscillator strengths of 1.345 and 1.915 are localized at 887 and 546 nm for the FPR14 molecule. Thus FPR14 has intense absorption at the visible and far-infrared regions, making it an ideal candidate for applications in solar energy collection. It is worth mentioning that Zhang and Antonietti have experimentally reported that g-C_3N_4 exhibits the photovoltaic effect and is potentially promising as photoactive material in converting solar light into electricity.[59]

IV. CONCLUSION

We have investigated the phase transitions of the molecular structures of cyanoacetylene, H−C≡C−C≡N, under pressures from 0 to 55 GPa by using first-principles simulations. It is observed that under pressure, the polar and nonpolar crystals of cyanoacetylene attain several first-order transitions from molecular form → polyacrylonitrile (PA) polymer → a polymer with fused pyridine rings (FPR's) → 3D structure. All these phase transitions are simultaneous with sudden contractions of volumes. At ambient pressure, the PA polymers have a helical-like shape and FPR polymers are curved. However, it is still possible to connect the FPR polymers to the metal electrodes for electronic applications. We used the nonequilibrium Green's function and time-dependent density functional theory techniques to consider the electron transport and optical characteristics of FPR polymers consisting of different numbers of rings (different length). It is observed that FPR polymers have NDR behavior under applied bias voltages and can absorb visible light efficiently. It is expected that the FPR polymers will be a good material for optoelectronic applications.

ACKNOWLEDGMENTS

The authors sincerely thank the crew of the Center for Computational Materials Science of the Institute for Materials Research, Tohoku University, for their continuous support of the supercomputing facilities. M.K. thanks the Japan Society for the promotion of Science (JSPS) for financial support.

*Author to whom all correspondence should be addressed. Present address: National Institute for Materials Science (NIMS), 1-1 Namiki, Tsukuba 305-0044, Japan; khazaei.mohammad@nims.go.jp

[1] S. C. Veenstra, J. Loos, and J. M. Kroon, Prog. Photovolt: Res. Appl. **15**, 727 (2007).
[2] T. Yamabe, S. Yata, and S. Wang, Synth. Met. **137**, 949 (2003).
[3] F. Marchioni, J. Yang, W. Walker, and F. Wudl, J. Phys. Chem. B **110**, 22202 (2006).
[4] S. Yata, E. Okamoto, H. Satake, H. Kubota, M. Fujii, T. Taguchi, and H. Kinoshita, J. Power Sources **60**, 207 (1996).
[5] J. P. Berffield, G. C. Solomon, C. A. Stafford, and M. A. Ratner, Nano Lett. **11**, 2759 (2011).
[6] S.-H. Ke, W. Yang, S. Curtarolo, and H. U. Baranger, Nano Lett. **9**, 1011 (2009).
[7] B. Biel, X. Blase, F. Triozon, and S. Roche, Phys. Rev. Lett. **102**, 096803 (2009).
[8] A. R. Rocha, V. M. Garca-Suárez, S. W. Bailey, C. J. Lambert, J. Ferrer, and S. Sanvito, Nature (London) **4**, 335 (2005).
[9] R. Firouzi and M. Zahedi, J. Mol. Struct., THEOCHEM **862**, 7 (2008).
[10] J. E. Norton and K. N. Houk, J. Am. Chem. Soc. **127**, 4162 (2005).
[11] P. J. Nigrey, A. G. MacDiarmid, and A. J. Heeger, J. C. S. Chem. Commun. 594 (1979).
[12] K. N. Houk, P. S. Lee, and M. Nendel, J. Org. Chem. **66**, 5517 (2001).
[13] J. M. André, B. Champagne, E. A. Perpète, and M. Guillaume, Int. J. Quantum Chem. **84**, 607 (2001).
[14] V. Schettino and R. Bini, Phys. Chem. Chem. Phys. **5**, 1951 (2003).
[15] E. K. Sichel, M. F. Rubner, and S. K. Tripathy, Phys. Rev. B **26**, 6719 (1982).
[16] D. B. Tanner, G. L. Doll, A. M. Rao, P. C. Eklud, G. A. Arbuckle, and A. G. MacDiarmid, Synth. Met. **141**, 75 (2004).
[17] M. Springborg, J. Am. Chem. Soc. **121**, 11211 (1999).
[18] M. Springborg, J. Mol. Struct., THEOCHEM **593**, 155 (2002).
[19] M. Springborg, Synth. Met. **135-136**, 347 (2003).
[20] M. Springborg, Chem. Phys. Lett. **339**, 389 (2001).
[21] J. E. Anthony, Chem. Rev. **106**, 5028 (2006).
[22] J. Roncali, Chem. Rev. **97**, 173 (1997).
[23] K. Aoki, Y. Kakudate, M. Yoshida, S. Usuba, and S. Fujiwara, J. Chem. Phys. **91**, 778 (1989).
[24] J. P. Perdew, K. Burke, and M. Ernzerhof, Phys. Rev. Lett. **77**, 3865 (1996).
[25] N. Troullier and J. L. Martins, Phys. Rev. B **43**, 1993 (1991).
[26] P. Ordejón, E. Artacho, and J. M. Soler, Phys. Rev. B **53**, R10441 (1996).
[27] J. M. Soler, E. Artacho, J. D. Gale, A. García, J. Junquera, P. Ordejón, and D. Sánchez-Portal, J. Phys. Condens. Matter **14**, 2745 (2002).
[28] D. Sánchez-Portal, E. Artacho, and J. M. Soler, J. Phys. Condens. Matter **8**, 3859 (1996).
[29] H. J. Monkhorst and J. D. Pack, Phys. Rev. B **13**, 5188 (1976).
[30] M. Khazaei, M. N. Tripathi, and Y. Kawazoe, Phys. Rev. B **83**, 134111 (2011).
[31] M. Khazaei, Y. Liang, M. S. Bahramy, F. Picherri, K. Esfarjani, and Y. Kawazoe, J. Phys. Condens. Matter **23**, 405403 (2011).
[32] F. Zahariev, S. V. Dudiy, J. Hooper, F. Zhang, and T. K. Woo, Phys. Rev. Lett. **97**, 155503 (2006).
[33] W. D. Mattson, D. Sanchez-Portal, S. Chiesa, and R. M. Martin, Phys. Rev. Lett. **93**, 125501 (2004).
[34] Atomistix ToolKit version 2008.10, QuantumWise A/S [www.quantumwise.com].
[35] M. Brandbyge, J. L. Mozos, P. Ordejón, J. Taylor, and K. Stokbro, Phys. Rev. B **65**, 165401 (2002).
[36] J. Taylor, H. Guo, and J. Wang, Phys. Rev. B **63**, 245407 (2001).
[37] M. J. Frisch, G. W. Trucks, H. B. Schlegel, G. E. Scuseria, M. A. Robb, J. R. Cheeseman, G. Scalmani, V. Barone, B. Mennucci, G. A. Petersson, H. Nakatsuji, M. Caricato, X. Li, H. P. Hratchian, A. F. Izmaylov, J. Bloino, G. Zheng, J. L. Sonnenberg, M. Hada, M. Ehara, K. Toyota, R. Fukuda, J. Hasegawa, M. Ishida, T. Nakajima, Y. Honda, O. Kitao,

H. Nakai Jr., T. Vreven, J. A. Montgomery, J. E. Peralta, F. Ogliaro, M. Bearpark, J. J. Heyd, E. Brothers, K. N. Kudin, V. N. Staroverov, R. Kobayashi, J. Normand, K. Raghavachari, A. Rendell, J. C. Burant, S. S. Iyengar, J. Tomasi, M. Cossi, N. Rega, J. M. Millam, M. Klene, J. E. Knox, J. B. Cross, V. Bakken, C. Adamo, J. Jaramillo, R. Gomperts, R. E. Stratmann, O. Yazyev, A. J. Austin, C. Pomelli, J. W. Ochterski, R. L. Martin, K. Morokuma, V. G. Zakrzewski, G. A. Voth, P. Salvador, J. J. Dannenberg, S. Dapprich, A. D. Daniels, O. Farkas, J. B. Foresman, J. V. Ortiz, J. Cioslowski, and D. J. Fox, *Gaussian 09, Revision A.02* (Gaussian, Inc., Wallingford, CT, 2009).

[38] M. Ernzerhof and G. E. Scuseria, J. Chem. Phys. **110**, 5029 (1999).

[39] C. Adamo and J. Barone, J. Chem. Phys. **110**, 6158 (1999).

[40] D. Jacquemin, E. A. Perpéte, G. E. Scuseria, I. Ciofini, and C. Adamo, J. Chem. Theory. Comput. **4**, 123 (2008).

[41] A. A. Westenberg and E. B. Wilson Jr., J. Am. Chem. Soc. **97**, 199 (1950).

[42] F. V. Shallorss and G. B. Carpenter, Acta Crystallogr. **11**, 490 (1958).

[43] See Supplemental Material at http://link.aps.org/supplemental/10.1103/PhysRevB.85.054101 for the coordinates of the predicted structures and the xyz trajectory files of phase transitions.

[44] M. Durandurdu, Phys. Rev. B **75**, 235204 (2007).

[45] K. Mizushima, S. Yip, and E. Kaxiras, Phys. Rev. B **50**, 14952 (1994).

[46] X.-D. Wen, R. Hoffmann, and N. W. Ashcroft, J. Am. Chem. Soc. **133**, 9023 (2011).

[47] X.-D. Wen, L. Hand, V. Labet, T. Yang, R. Hoffmann, N. W. Ashcroft, A. R. Oganov, and A. O. Lyakhov, Proc. Natl. Acad. Sci. (USA) **108**, 6833 (2011).

[48] J. Sun, D. D. Klug, C. J. Pickard, and R. J. Needs, Phys. Rev. Lett. **106**, 145502 (2011).

[49] J. Sun, D. D. Klug, R. Martonak, J. A. Montoya, M.-S. Lee, S. Scandolo, and E. Tosatti, Proc. Natl. Acad. Sci. (USA) **106**, 6077 (2009).

[50] A. Salamat, K. Woodhead, P. F. McMillan, R. Q. Cabrera, A. Rahman, D. Adriaens, F. Cora, and J. P. Perrillat, Phys. Rev. B **80**, 104106 (2009).

[51] E. Horvath-Bordon, R. Riedel, P. F. McMillan, P. Kroll, G. Miehe, P. A. van Aken, A. Zerr, P. Hoppe, O. Shebanova, I. McLaren, S. Lauterbach, E. Kroke, and R. Boehler, Angew. Chem. Int. Ed. **46**, 1476 (2007).

[52] H.-Y. Yan, Q. Wei, B.-B. Zheng, and P. Guo, J. Solid State Chem. **184**, 572 (2011).

[53] F. Brich, Phys. Rev. **71**, 809 (1947).

[54] S. Grimme, J. Comput. Chem. **27**, 1787 (2006).

[55] J. M. Seminario, A. G. Zacharias, and J. M. Tour, J. Am. Chem. Soc. **121**, 411 (1998).

[56] Y. Y. Liang, H. Chen, H. Mizuseki, and Y. Kawazoe, J. Chem. Phys. **134**, 144113 (2011).

[57] Y. Y. Liang, F. Jiang, Y. X. Zhou, H. Chen, R. Note, H. Mizuseki, and Y. Kawazoe, J. Chem. Phys. **127**, 084107 (2007).

[58] N. S. Venkataramanan, A. Suvitha, H. Nejo, H. Mizuseki, and Y. Kawazoe, Int. J. Quantum Chem. **111**, 2340 (2011).

[59] Y. Zhang and M. Antonietti, Chem. Asian J. **5**, 1307 (2010).